NEURAL DROPS : DATA DRIVEN DISCOVERY OF SOLUTE DEPENDENT DROPLET EVAPORATION DYNAMICS

Michael Machold†
Mechanical Engineering and Applied Mechanics
University of Pennsylvania
Philadelphia, PA 19104
mmachold@seas.upenn.edu

Benjamin D. Shaffer†
Mechanical Engineering and Applied Mechanics
University of Pennsylvania
Philadelphia, PA 19104
ben31@seas.upenn.edu

December 19, 2024

ENM 5310 Final Project, Fall 2024
Code for this project is available at https://github.com/bdshaffer31/NeuralDrops
†: *contributed equally*

ABSTRACT

Understanding the dynamics of evaporating droplets is essential in applications ranging from inkjet printing to microfluidics. This work presents a hybrid modeling approach to simulate the evolution of an evaporating drop, combining physics-based and data-driven methods. The finite difference method was implemented to model the changing height profile based on simplified Navier-Stokes equations. A Fourier Neural Operator based neural network was constructed to learn a functional mapping from droplet height to the evaporation rate. The numerical flow model and learned evaporation model are integrated within a Neural ODE framework to evolve the droplet state in time, altogether known as the Neural Drop Operator (DrOps) method. The proposed approach balances the interpretability of analytical methods with the adaptability of machine learning, allowing for accurate simulation of both single- and multi-component droplets. We demonstrate the efficacy of this approach by comparing predicted drop evolutions from learned models to experimental data. The Neural DrOps architecture exhibits similar or improved performance when compared to architectures like FNO (without physics) and Neural ODE. Neural DrOps has the additional benefit of decoupling intractable physics (multi-component evaporative flux) from fields of interest (velocity, concentration, and temperature) that cannot be interrogated in pure data-driven architectures.

1 Introduction

Multi-component drops have gained research interest due to a rise in applications that leverage flow and deposition of solutes contained inside volatile liquids. Growing research in microelectronics and micro-fluidics has led to technologies that leverage colloidal deposition for applications like ink-jet printing, biomedical sensing, and nano-scale fabrication processes [1]. Yet, there remains ample opportunity to model and identify new phenomena of solute deposition by tuning drop composition, system properties, and evaporation parameters that may unlock future micro and nano-scale devices.

Multi-component drops consist of one or more solutes mixed in one or more solvents. The flows induced by the interplay of solutes and the evaporating solvents plays a crucial role in the deposition pattern of solutes. This process is a complex multi-physics problem that couples a moving boundary with the flow of gases outside the drop as well as flows induced by temperature and concentration inside the drop [2]. Active research is being conducted to experimentally control deposition formation by architecting substrates to control drop shape through surface properties or tailoring drop composition through the use of surfactants and multiple solvents [3].

To aid in the probing of system parameters that control deposition, various modeling approaches have been de-

veloped to elucidate the general physics governing multi-component drop evaporation. While these numerical modeling approaches have led to the identification of various flow phenomena, the complexity of component interaction limits the applicability and accessibility of numerical models for all multi-component drop applications. For multi-component systems, evaporation rates depend on the individual volatilities of the components, their activity coefficients, and potential Marangoni flows induced by surface tension gradients. These effects are challenging to capture analytically, especially when the droplet composition changes dynamically over time.

To address these complexities, we propose as data-driven approach to model evaporation using Fourier Neural Operators (FNOs). In our approach, FNOs provide an efficient framework for learning mapping from the drop state to the evaporation rate. This is coupled with a PDE solver leveraging the finite difference method to track the development of flow during evaporation. The combined analytic fluid model and learned flux model are integrated within a neural ODE framework. We refer to this method as the Neural Drop Operator (DrOps) This provides a physics based digital twin for modeling the evolution of an evaporating drop containing polymer solute. Our unique framing of the droplet modeling problem as a data driven inverse problem for flux modeling allows generalization to complex solutes and drop geometries such as polymers, and can be used to guide experimental design as well and manufacturing processes.

2 Problem statement

The liquid air-interface of a low-contact angle sessile droplet Γ can be expressed in Monge's form [4],

$$\Gamma(t) = \{(r, z)|z = h(r, t)\} \tag{1}$$

where $h(r, t)$ represents the height profile of the droplet over a one-dimensional domain $r \in \Omega$ at time $t \in [0, T]$, with total mass,

$$M = 2\pi\rho \int_0^R rh(r)\,\mathrm{d}r. \tag{2}$$

Changes in the height are a result of both interior flow and evaporation,

$$\frac{\mathrm{d}h}{\mathrm{d}t} = \mathcal{Q}(h) - \mathcal{E}(h), \tag{3}$$

where $\mathcal{Q}$ captures the change in height profile due to redistribution of fluid mass within the drop and $\mathcal{E}$ is the mass flux at the interface. The internal flow, $\mathcal{Q}$, must satisfy

$$0 = \int_\Omega \mathcal{Q}\,\mathrm{d}V = \int_0^R r\mathcal{Q}(r)\,\mathrm{d}r, \tag{4}$$

as conservation of mass, while the evaporation, $\mathcal{E}$, must describe a positive mass flux from the droplet into the surrounding air

$$\dot{M}_{air} = -\dot{M}_{drop} = \int_\Gamma \mathcal{E}\,\mathrm{d}S = \int_0^R r\mathcal{E}(r)\,\mathrm{d}r \geq 0. \tag{5}$$

We express the state of the drop profile as an initial value problem

$$h(r, t+\Delta t) = h(r, t_0) + \int_{t_0}^{t+\Delta t} [\mathcal{Q}(h, r, \tau) - \mathcal{E}(h, r, \tau)]\,\mathrm{d}\tau \tag{6}$$

Given the height profile $h(r, t)$ and a set of conditioning variables z (e.g., temperature, concenration, or surface properties) at time t, we propose to approximate the surface mass flux $\mathcal{E}(r, t)$ as:

$$\mathcal{E}(r, t) = f_\theta(h(r, t), z) \tag{7}$$

where f_θ represents the FNO model parameterized by learnable weights θ. The conditioning variables z allow the model to adapt to different physical scenarios, capturing the effects of varying environmental and material properties.

2.1 Contributions

This work introduces a hybrid modeling approach that combines the strengths of physics-based and data-driven methods to simulate droplet evaporation dynamics. The key contributions include:

- **Integration of FNOs with Neural ODEs:** We propose a novel integration where the mass flux due to evaporation is modeled using an FNO, capturing complex, spatially varying evaporation patterns. This FNO is embedded within a Neural ODE framework that governs the temporal evolution of the droplet's height profile.
- **Hybrid Modeling of Droplet Dynamics:** The internal flow within the droplet is described numerically using the thin film approximation of the Navier-Stokes equations, while the evaporation flux is learned from data using the FNO. This combination allows for accurate and efficient simulation of droplet behavior, balancing interpretability and flexibility.
- **Interpretability of Learned Mass Flux:** By framing the learnable model as a mass flux term, our approach allows for direct physical interpretation of the learned behavior. Unlike black-box solution operator methods, which provide limited insight into the underlying dynamics, our model's outputs correspond to physically meaningful quantities. This interpretability bridges the gap between data-driven learning and domain knowledge, enhancing trust and applicability in scientific and engineering contexts.

3 Background

3.1 Analytical Expressions for Evaporative Mass Flux

Evaporative mass flux on the drop surface induces flows inside the drop that lead to interesting solute behavior. For

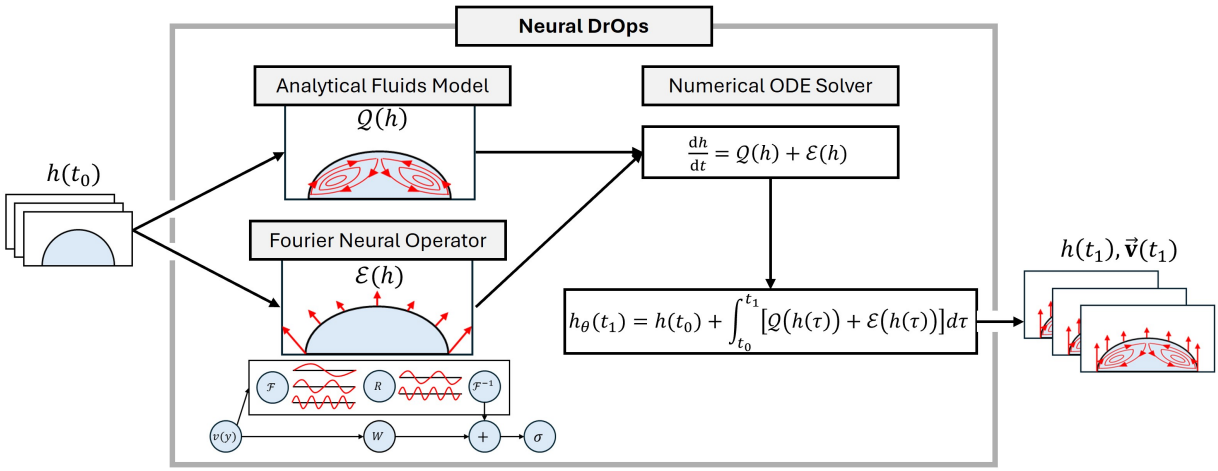

Figure 1: Flow chart depicting lubrication approximation driven finite differences method coupled with machine learned model of evaporative flux. This coupled model is passed through a numerical ODE solver to predict the height history, velocity fields, and evaporation.

a pure drop with diffusion limited evaporation (i.e. water), this evaporative flux has been approximated by analytical expressions [5, 6]. As the contact angle between a drop and a solid substrate decreases, the relative evaporation at the contact line increases, inducing capillary flow that drives mass to the contact line. The validity of this analytical expression has since been corroborated by experimental and numerical investigations [6].

Additional work has been conducted to make analytical models of various solvents taking into account the role of temperature, ambient conditions, and chemical activity of evaporated solvents [7]. An evaporation model that considers the role of drop composition was developed by Guena et al. [8] in which it was shown that the volatility of each component effects the evaporation along the entire drop surface. The application of this concentration dependent evaporation model was shown to agree well with experimental measurements of drop height history for binary mixtures [4]. Such analytical expressions give insight into the complexity and importance of evaporation, but do not give insight into the coupled velocity, concentration, and temperature fields that arise inside the drop.

3.2 Numerical Modeling of Multi-Component Drops

Concentration of solutes in a drop evolve with the temperature dependent flow fields induced by evaporation and the inhomogeneous properties of the mixture. The evolution of mass, energy, and momentum inside of a drop present a coupled multi-physics problem in which various non-linear partial differential equations must be solved.Various numerical models have been developed to obtain solutions to this problem, ranging from molcular dynamics (MD) simulations at the finest scales [3] to FEM leveraging arbitrary Euler-Lagrangian boundaries [9].

In Bhardwaj et al. a finite element scheme was developed to model ring-like deposits in a two-component drop [10]. This scheme was setup in a Lagrangian framework to track fluid movement with the full Navier-Stokes equation. In addition, a re-meshing scheme was introduced to account for the pinning and evolution of the contact line in the presence of a forming deposit. Similar numerical simulations have leveraged various finite element models with arbitrary Euler-Lagrangian [11] PDE formulations or alternative moving mesh schemes [9]. These approaches can be highly accurate but are computationally expensive, and require knowledge about both the chemical activity within the droplet and in the surrounding air to track the evaporation of solvents.

Substantial work has been done to produce a simplified model, particularly in the limit of thin, low contact angle drops. Diddens et al. developed a finite volume based model, that leveraged the lubrication approximation, with the ability to simulate multi-component drops [4]. In this model, the concentration and velocity profiles within the drop were tracked and used to update concentration dependent properties like viscosity, surface energy, and density. This model predicted drop geometry evolution that matched experiments for pure drops, water/ethanol drops, and water/glycerol drops. This model predicted phenomena like solvent replenishment by solutal Marangoni flow in water/ethanol drops, as well as polymer skin formation in water/glycerol drops. While these models are useful due to their relative simplicity, they fail to capture the full range of multi-component droplet dynamics and are constrained in geometry by the lubrication approximation.

From the analytical and numerical modeling of drops, many predictions can be made about the evolution of drops and the resulting deposition. Yet, for many drop compositions these models require extensive understanding of concentration dependent properties. In addition, the non-

linear PDEs that result from such properties make many models computationally expensive to run and experimentally intense to validate.

3.3 Related Works

Our approach combines knowledge based learning, neural operators, and neural differential equations to model evaproative mass flux in multi-component sessile droplets. We briefly review related works both in terms of method and application.

3.3.1 Related methods

In recent years, a growing body of research has focused on integrating physical structure into machine learning models for scientific applications, motiviated by the successes of Raissi et al. [12]. Several physics-informing architectures have been proposed in the context of neural ODEs, such as Lai et al. (2021) [13], who introduce a method for structural identification. In their approach, the neural network is trained to satisfy physical constraints by incorporating them into the loss function. Similarly, Sholokhov et al. (2023) [14] propose the Physics-Informed Neural ODE (PINODE) method, which uses collocation points to enforce PDE constraints during training. Jiahao et al. [15] provide a general framework for incoporating prior knowledge in neural ODES (KNODEs).

Operator regression has proved an effective method for learning data driven digital twins of physical systems, however these methods most commonly learn the solution operator directly. Cho et al. (2024) [16] explore the integration of operator-learning-inspired methods with Neural ODEs, proposing a general framework where operator learning enhances the expressiveness of Neural ODEs.

Verma et al. [17] structure their model as a learnable flux network for advection diffusion problems specifically tailored for climate modeling. Kim and Kang use FNOs to parameterize hyperbolic conservation laws [18]. Patel et al. (2021) [19] propose a physics-informed operator regression framework to learn continuum models directly from data while respecting underlying physical laws. Actor et al. (2024) [20] introduce a data-driven approach utilizing Whitney forms for structure-preserving control volume analysis, ensuring that machine learning models respect geometric and topological constraints inherent in physical systems.

Our Neural DrOps method uniquely integrates concepts from across these methods to learn a flux term within a Neural ODE framework, enabling a physically interpretable simulation of the coupled internal flow and evaporation dynamics in sessile droplets.

3.3.2 Machine learning for drops

Machine learning applications for sessile droplet evaporation predominantly aim to streamline experimental processes, reduce the frequency and extent of measurements, and expedite computational analyses [21, 22, 23]. Lashkaripour et al. (2021) [21] developed an ML-based framework for optimizing droplet formation parameters in microfluidic flow-focusing devices, enhancing design automation. Arnov and Dhar (2024) [22] employed deep networks and tree-based models to predict sessile droplet evaporation kinetics, emphasizing accurate evaporation prediction from experimental data. Andalib et al. (2021) [23] proposed a data-driven method for state estimation of evaporating droplets, using ML to infer interface dynamics from limited observations. The PINNs4Drops framework [24] employs a combination of Physics-Informed Neural Networks (PINNs) and Convolutional Neural Networks (CNNs) to reconstruct two-phase flow dynamics from experimental image data, specifically targeting gas-liquid interface evolution. These models are primarily concerned with isolated outcomes, such as parameterized evaporation rates or final deposition profiles, rather than providing a holistic representation of the complex, nonlinear dynamics inherent in droplet evaporation.

3.4 Neural Ordinary Differential Equations

Neural Ordinary Differential Equations (NODEs) [25] can be viewed as a continuous-time generalization of Residual Networks (ResNets). In the limit of an infinite number of infinitesimally small layers, the ResNet update, $h_{n+1} = h_n + f_\theta(h_n)$, becomes a continuous differential equation, $\dot{h} = f_\theta(h(t), t)$. This formulation defines a Neural ODE, where the evolution of $h(t)$ is modeled as a continuous trajectory through the feature space. Given an initial state $h(t_0)$, the solution at a later time t is obtained by numerically integrating this differential equation. In practice, this integration is performed using standard numerical ODE solvers, such as Runge-Kutta methods, allowing for adaptive step sizes and continuous-time evaluations.

In the context of this project, Neural ODEs are used to model the continuous evolution of the droplet height profile $h(r, t)$ over time according to the internal flow and model evaporation.

3.5 Neural Operators

Neural operators [26, 27] represent a generalization of neural networks designed to learn mappings between function spaces, making them suitable for problems involving partial differential equations (PDEs) and other continuous-domain tasks. Unlike traditional neural networks that map finite-dimensional inputs to finite-dimensional outputs, neural operators approximate mappings between infinite-dimensional spaces, enabling resolution-invariant predictions. Formally, a neural operator learns a mapping $\mathcal{G} : \mathcal{U} \mapsto \mathcal{V}$ where $\mathcal{U}$ and $\mathcal{V}$ are function spaces. For an input function u defined over a domain D, the neural operator outputs a function $v = \mathcal{G}(u)$, where $u : D \mapsto \mathbb{R}^d$ and $v : D \mapsto \mathbb{R}^k$.

A specialized class of neural operators, the Fourier Neural Operator (FNO), achieves efficiency by leveraging the Fast Fourier Transform (FFT) to capture global dependencies in the data. The key idea of the FNO is to perform linear transformations in the Fourier domain, where long-range correlations can be represented more effectively than in the spatial domain. Given an input function $u(x)$, defined on a domain $x \in \mathbb{R}^d$, an FNO layer applied the following operations: first, the Fourier transform $\mathcal{F}(u)$ maps the input to the frequency domain, resulting in $\hat{u} = \mathcal{F}(u)$. A learnable linear transformation R is then applied in Fourier space, yielding $\hat{v} = R \cdot \hat{u}$. The inverse Fourier transform $\mathcal{F}^{-1}$ maps back to the spatial domain, producing $v = \mathcal{F}^{-1}(\hat{v})$. To incorporate non-linearity and local interactions, a residual connection and a point-wise linear transformation W are added, followed by a non-linear activation function σ, resulting in the final output:

$$v = \sigma(\mathcal{F}^{-1}(R \cdot \mathcal{F}(u)) + W(u)). \tag{8}$$

By learning in Fourier space, the FNO method efficiently models global interactions while maintaining resolution invariance. This makes FNOs particularly suitable for solving PDEs and modeling physical systems where complex spatial and temporal dependencies are present. Their applications span various fields, including fluid dynamics, weather prediction, and engineering simulations. By combining the expressiveness of neural networks with the efficiency of FFT-based operations, FNOs offer a powerful framework for learning mappings between function spaces in a computationally efficient manner.

Neural operators are most commonly used to directly approximate the *solution* operator of PDEs. Given a PDE $\mathcal{N}(u(x)) = f(x)$, this entails learning the mapping from the input function $f(x)$ to the solution function $u(x)$, as $\mathcal{G}_\theta : f(x) \mapsto u(x)$. In this work, we instead utilize neural operators to learn a continuous flux operator where, i.e. $u(x)$ is the mass flux function. By combining this with a neural ODE and analytic flow model we obtain a model which is continuous in space and time and are able to obtain state estimations while directly parameterizing the unknown flux function.

4 Physical Drop Model

We consider a one-dimensional droplet model derived from a lubrication approximation of the Navier Stokes equations [4] [28]. The model describes the dynamics of thin, axisymmetric sessile droplets with small contact angles, and captures the essential physical processes, including curvature-driven capillary flow, surface tension gradients (Marangoni effects), and evaporation-induced changes in the droplet profile. The evaporation is assumed to be diffusion-limited, with the local evaporation rate determined by the vapor concentration gradient at the liquid-air interface. The drop description is shown schematically in figure 3.

4.1 Flow model

To model the liqud flow within the drop we consider a simplified version of the lubrication approximation model developed by Diddens et al. for modeling multi-component drops [4]. We simplify this model for the special case of a pure drop, with constant viscosity, density, and surface tension, resulting in a equivalent model to the thin film approximation presented by Siregar et al [28], but with the inclusion of velocity field computations.

The lubrication approximation assumes a flat drop, and therefore small contact angle, θ, as well as low Reynolds number. Gravitational forces are neglected based on the relative size of the drop and capillary length, and the flow is treated in the steady limit [4].

Applying these approximations to the Navier Stokes equations with applicable boundary conditions results in an evaporation-free model for the drop profile,

$$\frac{\partial h}{\partial t} = -\frac{1}{r}\frac{\partial}{\partial r}\int_0^h r\boldsymbol{u}\,\mathrm{d}z, \tag{9}$$

where u corresponds to the radial velocity, $\boldsymbol{v} = \boldsymbol{u}\hat{e}_r + \boldsymbol{w}\hat{e}_z$. The radial velocity is determined by both pressure induced capillary flow and surface tension induced Marangoni flow,

$$\boldsymbol{u}(r,z,t) = \int_0^z \left[-\frac{\partial p}{\partial r}(h(r,t) - z') + \frac{\partial \sigma}{\partial r}\right]\mathrm{d}z', \tag{10}$$

where σ is the surface tension. For the case of a pure drop with constant ambient and substrate temperature, Marangoni flow can be safely neglected [29]. The Laplace pressure in 12 is based on the curvature of drop surface,

$$\kappa = \frac{r\partial_r h}{\sqrt{1 + (\partial_r h)^2}}, \tag{11}$$

for a pressure,

$$p = p_L = -\sigma\frac{1}{r}\frac{\partial \kappa}{\partial r}. \tag{12}$$

The $\boldsymbol{w}$ velocity can be determined from conservation of mass for visualization.

4.2 Evaporation model

To numerically simulate the evaporation of pure droplets, an analytical model of the evaporative flux is adopted from literature [5]. For this model it is assumed that the drop consists of a single solvent that follows diffusion-limited evaporation (i.e water).

Following the model of Deegan et al. [5], the gradient of concentration in the air surrounding the drop is determined by solving the Laplace equation in the region bounded by

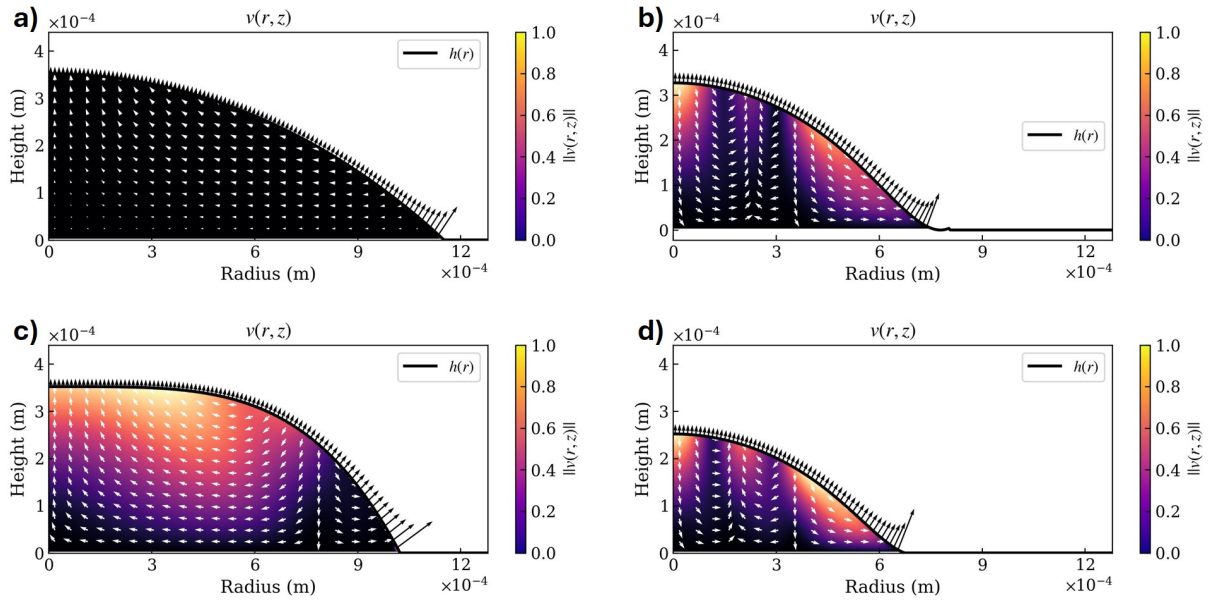

Figure 2: Predicted internal flow fields simulated using the numerical model and an analytical expression for evaporation. Flow fields are induced by drop geometry and imposed evaporation ($\mathcal{E}(h)$). Plots shown for an initialized geometry of a spherical cap at a)$t = 0[s]$ and b)$t = 16[s]$. An initialization of a quartic parabolic drop at c)$t = 0[s]$ and d)$t = 32[s]$. Direction of internal velocity is indicated by white arrows.

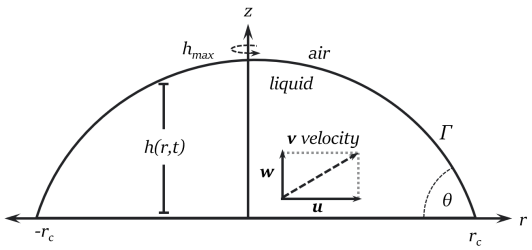

Figure 3: Drop schematic, inspired by [4].

the drop profile, substrate, and a large region of surrounding air ($r \to \infty$). The solution to this boundary value problem can be approximated by an analytical expression that varies with contact radius (R_c) and contact angle (θ). An approximation of diffusion-limited evaporation along the droplet is given by

$$J(r) = \frac{D_{vap} c_{sat} (1 - RH)}{c_l R_0} \left(\frac{1}{1 - r/R_c}\right)^{\frac{\pi - 2\theta}{2(\pi - \theta)}} \tag{13}$$

Where the flux is dependent on the saturation concentration (c_{sat}), relative humidity (RH), vapor diffusivity (D_{vap}), and concentration of liquid water (c_l). As the contact angle decreases, the evaporative flux enhancement at the corner becomes greater.

From these mass flux solutions, the evaporative velocity of solvent vapor along the interface is found using

$$\mathcal{E} = w_e = -\frac{J}{\rho}\sqrt{1 + \left(\frac{\partial h}{\partial r}\right)^2} \tag{14}$$

In the numerical model we add an $\varepsilon = 1e - 6$ constant evaporation for stability. A full description of this evaporation model can be found in the appendix.

5 Methods

5.1 Neural DrOps

The proposed Neural DrOps method parameterizes the droplet evaporation mass flux using a hybrid approach that combines a large constant evaporation term with a learnable correction. This correction term is modeled by a Fourier Neural Operator (FNO), enabling the capture of complex, spatially varying evaporation patterns. Physically, evaporation depends on the vapor concentration in the surrounding air, and therefore the solution to the Laplace equation as described in the appendix. Therefore, the evaporation model requires global information on the drop shape, such as in the FNO implementation, and can not be modeled only using local context such as in learned stencil approaches [30]. The mass flux $f_\theta(h, r)$ in equation 15 at position r is expressed as:

$$f_\theta(h, r) = |\kappa - \alpha f_{\theta, FNO}(h, r)| \tag{15}$$

where κ is a relatively large constant evaporation, and α is a tunable constant hyperparameter to help ensure numeri-

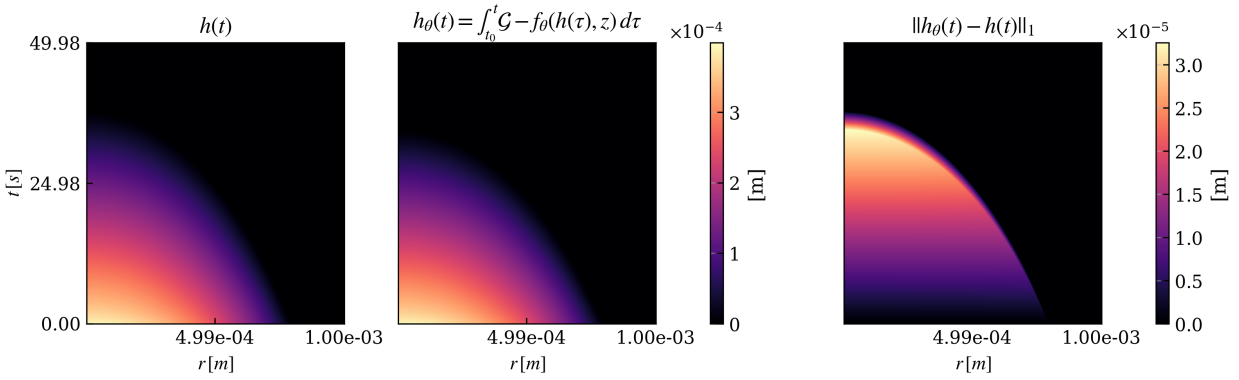

Figure 4: Comparison of drop height history for simulated spherical cap geometry and prediction from Flux FNO learned model. a) Data was generated by simulating an initial spherical cap profile with analytical flux model adapted from Deegan et al. [5]. b) Predicted height history from simulation initialized with the data and evolved with learned evaporative flux model. c) Relative error between input data and predicted output.

cal stability by appropriately scaling the model output at initialization. In all studies we use values of $\kappa = 1e-2$ and $\alpha = 1e-1$. When the modeled evaporation is smaller than the analytic evaporation, $f_\theta < w_e$, the numerical solution often becomes unstable. By initializing with an artificial large evaporation, $\kappa \gg w_e$, we help ensure the model approaches the solution from the stable direction.

To numerically solve equation 3 we discretize along the radius as r_i for $i = 1, 2, \ldots, N$ and height as z_i for $i = 1, 2, \ldots, M$, giving

$$\frac{\mathrm{d}h_i}{\mathrm{d}t} = \mathcal{Q}_i(h) - \mathcal{E}_i(h) \tag{16}$$

where the flow is modeled by equation 9

Exploiting the resolution invariant property of neural operators, a single model can be used across different discretization schemes arising from different data sources. This property allows for pretraining on large a dataset across available experiments and simulations with the opportunity to fine tune or run inference on the desired discretization.

The model predictions are generated by means of neural ODE coupled with the numerical flow model. This prediction is rolled out in time by a forward Euler solver from t_0 to t_1, and therefore requires a differentiable physics model for backpropagation. A forward pass of the model is:

$$h_\theta(t_1) = h(t_0) + \int_{t_0}^{t_1} \left[\mathcal{G}(h(\tau)) - f_\theta(h(\tau), z)\right] \mathrm{d}\tau \tag{17}$$

where the integration is handled by the ODE solver which iteratively calls the physics and flux models.

During training we specify a trajectory length, L, and construct the dataset as $\{h(t_i), [h(t_{i+1}), h(t_{i+2}), \ldots, h(t_{i+L})]\}_{i=1}^{T-L}$. We ensure the ODEINT in equation 17 collocates in time with the target data to compute the MSE loss.

$$\mathcal{L}(\theta) = ||h_\theta(r, t_i) - h(r, t_i)||_2^2 \tag{18}$$

We were not able to use the adjoint method for integrating the numerical ODE due to software constraints, resulting in a large memory cost for long training trajectory lengths; this is not a concern for inference.

To evaluate the learned model, we integrate the learned flux and internal flow from an initial drop profile $h(r, t = 0) = h_0$ through the experiment length giving $[h_{\theta,1}, h_{\theta,2}, \ldots, h_{\theta,T}]$. We compare this modeled drop profile history to the ground truth data and compute metrics such as MSE, contact line radius, and total volume.

5.2 Numerical Approach

We model equations 9, 10, 11, 12, using a second order finite difference scheme in one dimension for h, and two dimensions for $\mathbf{v}$. Where possible we replicated the model described in [4]. The resulting system of equations was solved by a forward Euler method with a constant step size. The numerical solver and physics model are entirely differentiable and parralelizable, allowing for seemless integration with machine learning training.

The numerical model is inherently unstable due to the high number of spatial derivatives required and physical singularities at the center and edge of the drop when not employing a precursor film. The moving interface poses a challenge for the velocity integral in equation 9, which was addressed by an immersed boundary method. A gaussian mollified derivative is used when taking the derivative of the $\mathbf{u}$ velocity integral to smooth out remaining discontinuities. While the to model was successful in handling simple geometric drop geometries, the irregularities in experimental data necessitated additional adaptation. To maintain a smooth profile during time integration, the interior height profile is projected on a low order polynomial after each step (n=8). The height profile of the drop is constrained to be non-negative after each solver step.

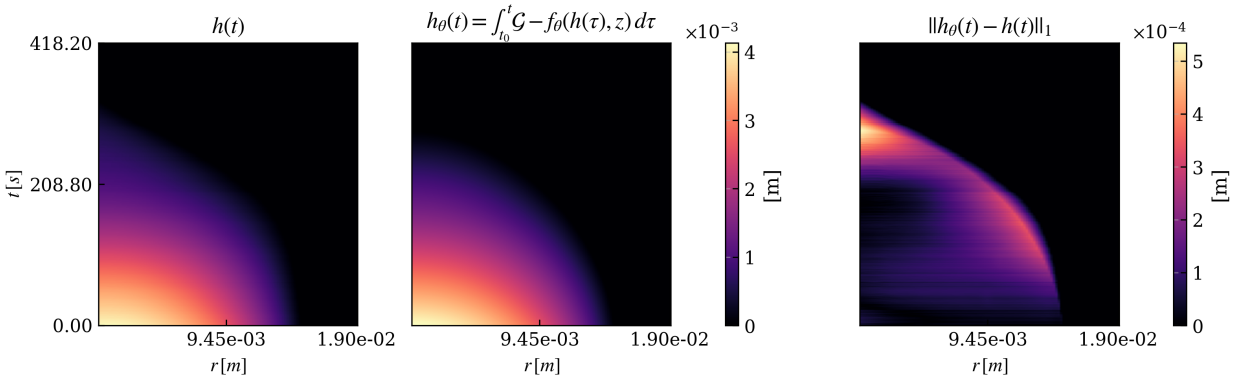

Figure 5: True drop height data in space-time and Neural DrOps modeled drop shape from initial condition only with absolute error.

While the problem formulation describes an axis-symmetric drop, for numerical stability we simulate both halves but constrain them to be axis symmetric. This prevents instabilities at the origin from enforcing the Neumann boundary condition. Accordingly, resulting $\dot{h}_t$ is scaled by $1/2$.

5.2.1 Verification

We verify the developed numerical method coupled with the analytical expression for evaporative flux adapted from Deegan et al. [5].

In figure 2, the flows of a spherical cap (a) and a quartic polynomial cap (c) at initialization and late in evaporation (b,d) are shown. From these flows, it can be seen that the constant Laplace pressure of a spherical cap leads to negligible predicted flow. Conversely, the geometry of the quartic cap boundary leads to non-uniform pressure throughout the drop and induces strong flow until the drop reaches a spherical cap shape. From both initialized geometries, the later stages of evaporation take on a spherical cap shape. Internal flows of the predicted spherical caps suggest strong mass transport to the contact line due to the high evaporative flux. The modeled internal flows resemble capillary flow in the absence of solutal or thermal Marangoni flow and qualitatively match the expected phenomena identified in literature [7].

6 Results

To evaluate the effectiveness of our proposed Neural DrOps method, we evaluate it in two experiments. The first using simulated data generated from the lubrication approximation flow model 9 with an analytic evaporation model. The Neural DrOps model directly incorporates the flow model explicitly, meaning we only need to learn the nonlinear evaporation term. We then evaluate the generalization capability of this method by evaluating it on several experimental datasets covering a range of conditions with multi-component drops. While the lubrication approximation applies as a first order approximation of the flow physics in this data, our implementation does not capture effects such as changes in viscosity and surface tension driven Marangoni flows that arise in multi-component drops. This experiment highlights how incorporating a data-driven flux term into the physical model allows for further generalization.

6.1 Experiment 1: simulated data

The Neural DrOps architecture was used to learn an evaporative flux model that predicts the height history of a given dataset. As an initial test, a dataset was generated by simulating the evolution of a spherical cap shape (see appendix for governing equation) with a prescribed evaporative flux given by the expression in section 4.2. The Neural DrOps was trained using this dataset with 90% allocated for training and 10% used for validation. The learned model was then used to predict the height history of the trained data. Figure 4 details the ground truth data and the predicted height history. Figure 4c shows the error between the predicted history and the actual history. It can be seen that the learned model correctly predicts the height history for a trajectory time of 16 seconds.

A height profile was extracted from the predicted history and the learned evaporative flux was used to simulate the flow patterns within the drop. Figure 6 shows internal flow patterns predicted from two time points along the trajectory. From the initial height profile, a stagnant flow pattern is predicted which can be expected based on the constant Laplace pressure of a stationary spherical cap. The flow at $t = 16[s]$ shows flow induced by the learned flow model.

In addition to the Neural DrOps model, two additional ML architectures were used to understand the impact of the hybrid model on flexibility and accuracy of model predictions. Three architectures were trained on data generated from the numerical model and predicted drop evolutions were compared to the ground truth for verification. Figure 7, shows that the MLP based Neural ODE produced the least accurate predictions with both FNO architectures yielding

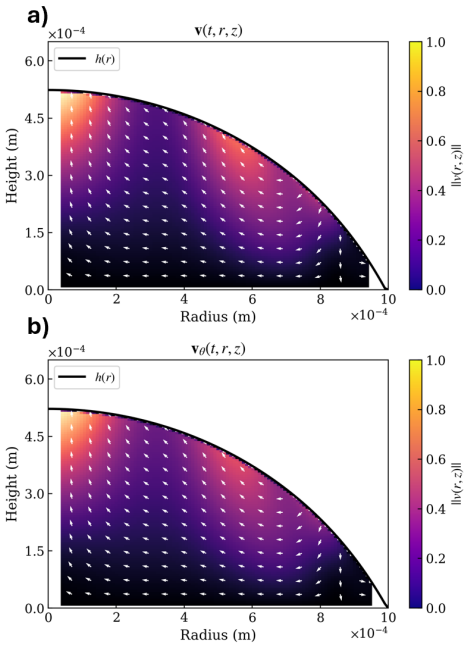

Figure 6: Modeled internal flow fields simulated using the numerical model and learned evaporation model.

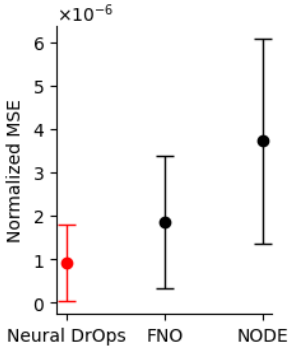

Figure 7: Comparison of proposed Neural DrOps method with solution operator FNO model and MLP based NODE model without physics.

a 2 to 3 times decrease in average MSE. When comparing the two FNO architectures, it can be seen that the Neural DrOps produced similar predictions to the architecture lacking the coupled numerical model.

6.2 Experiment 2: experimental data

We additionally evaluate the ability of the Neural DrOps method to handle experimentally collected data. The data were collected by imaging the profile of an evaporating water drop with cellulose nano-fibril (CNF) solute, and proccessing to extract the boundary height. This solute was chosen based on the complex rheological behavior of CNF in water. As the concentration of CNF increases, the viscosity increases by orders of magnitude. In addition, CNF is made up of long fibers that form a physically cross-linked porous matrix. Such a system suggests the analytical model of evaporative flux with concentration dependence [8] cannot easily be applied to this drop composition. The experimental process is described in appendix C.

As in the simulation experiment, we use the numerical pure drop model to simulate internal flows and model the evaporative flux with a trainable FNO. Notably, the flow in this multi-component drop deviates from the analytic pure drop model described in equation 9.

Figure 5 shows the modeled height and error. Overall, the Neural DrOps accurately reproduces the height profile over time, with error concentrated at the contact line and end of evaporation. Figure 8 shows the height profiles and modeled internal flows for the experimental data and modeled solution at time $t = 50\Delta t$. While the Neural DrOps model captures the expected drop shape, the internal flows have qualitative differences. The true profile results in multiple flow directions, both towards the contact line and towards the center of the drop, whereas the flow induced by the profile generated by the Neural DrOps model is on average faster and only oriented towards the drop center. This result may contribute to the differences at the boundary, since the internal flow directly affects the drop shape.

As in the simulated experiment, we compare the Neural DrOps model with a purely data driven FNO and MLP-based NODE model. The average MSE values for these models is shown in figure 9. Both FNO based approaches show relatively good performance. Unlike for the simulated data, directly modeling the solution is shown to be slightly more accurate. In cases where only a solution is desirable, this is a reasonable approach. However, for applications related to droplet dynamics, particularly those involving deposition modeling and control, an accurate evaporation model necessitates the use of the Neural DrOps architecture.

Drops are often characterized by contact line and total mass or volume. Figure 10 shows the modeled volume compared to the true volume. While the volume is accurately captured over time, the Neural DrOps model slightly overestimates the total evaporation, resulting in a lower volume. The evolution of the contact line is shown in

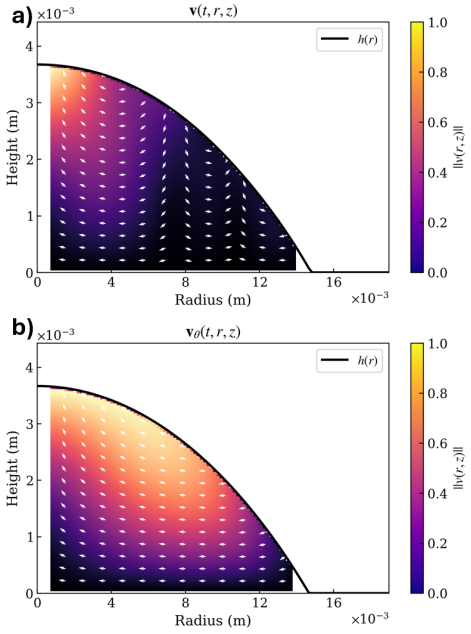

Figure 8: Modeled internal flow fields simulated using the numerical model and learned evaporation model.

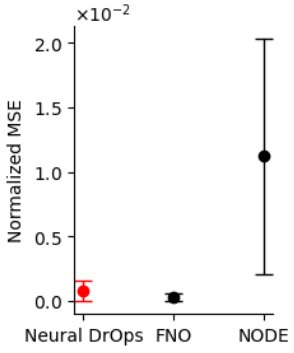

Figure 9: Comparison of proposed Neural DrOps method with solution operator FNO model and MLP based NODE model without physics.

figure 11. This experiment exhibited a receding contact line, and the Neural DrOps model accurately captures this phenomenon.

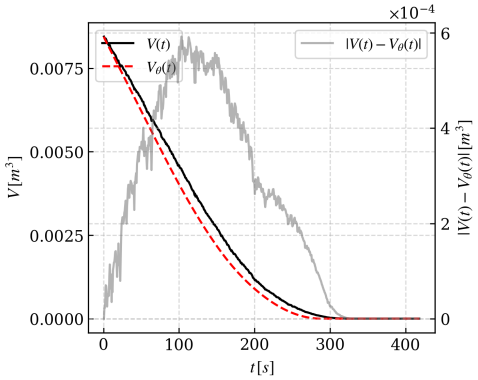

Figure 10: Total drop volume for measured data and Neural DrOps modeled solution.

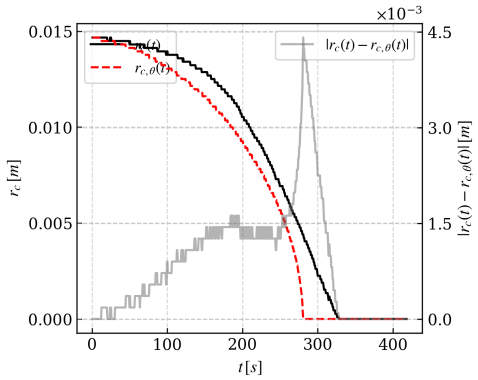

Figure 11: Progression of drop contact line over time for measured data and Neural DrOps modeled solution.

Finally, we visualize the learned flux based on the experimental data over time in figure 12. The learned flux results in the highest evaporation at the center of the drop and decreases with radius. This is a surprising result given that the analytic evaporation has a singularity at the contact line, and therefore the opposite trend is expected. Combined with the observation from figure 8 that the Neural DrOps model results in higher flow toward the center, suggests that this learned flux may be an artifact correcting for an inaccuracy of the flow term. This will be investigated in future work.

In addition to evaluating the Neural DrOps approach on a single experiment, we more broadly consider its generalization capability by evluating the prediction accuracy acrosss seven experimental datasets, all imaging multi-component CNF/water droplets at varying temperatures. We train a single model, conditioned on the temperature and demonstrate highly accurate prediction in figure 13. Additional visualizations of these results are provided in the appendix.

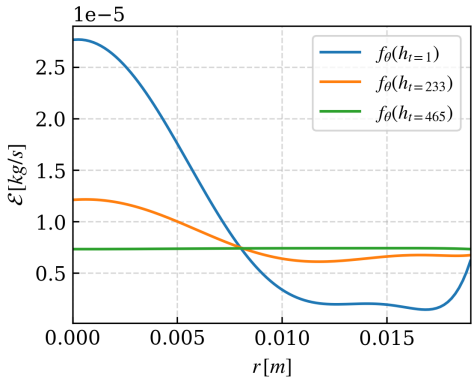

Figure 12: Visualization of learned flux term on experimental data.

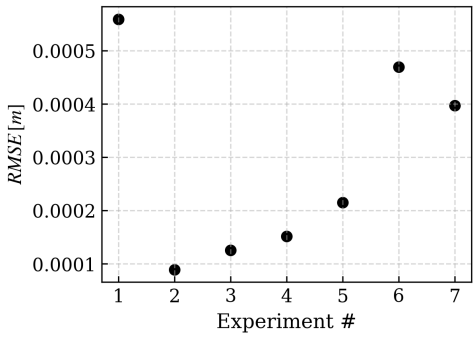

Figure 13: Average MSE for Neural DrOps evaluated on experimental datasets.

7 Conclusions

In this work, we presented Neural DrOps , a hybrid approach that integrates physics-based modeling with data-driven learning to simulate the evaporation dynamics of sessile droplets. By parameterizing the mass flux with a Fourier Neural Operator (FNO), combined with an analytic flow model within a Neural ODE framework, our method accurately captures the interplay between capillary-driven internal flow and complex evaporation patterns. The Neural DrOps model demonstrated competitive performance compared to conventional solution operator and Neural ODE models, achieving lower mean squared error (MSE) in both numerical simulations and comparable error in experimental validations. Furthermore, the learned flux term provides interpretability, offering insights into the spatial variability of the evaporation process, which distinguishes this approach from black-box alternatives.

Future work will focus on improving the efficiency and accuracy of the numerical solver used for the thin film equations by utilizing spectral methods. Additionally, we aim to evaluate the evolution of solute distribution within the drop to predict and control the deposition pattern. This will be achieved by implementing the continuity equation and conservation of energy to track concentration and temperature fields. These advancements have the potential to broaden the applicability of the Neural DrOps framework to areas such as micro-fluidics, ink-jet printing, and material deposition processes.

Acknowledgment

The authors thank Nat Trask, Kevin Turner, and Brooks Kinch for guidance on experimental design and development of the presented Neural DrOps methodology. This material is based upon work supported by the National Science Foundation Graduate Research Fellowship under Grant No. 2024371230.

Data Availability Statement

The described simulation and experimental data are available upon reasonable request.

References

[1] Khellil Sefiane. Patterns from drying drops. *Advances in Colloid and Interface Science*, 206:372–381, 2014.

[2] F. Giorgiutti-Dauphin´e and L. Pauchard. Drying drops. *European Physics Journal E*, 2018.

[3] Haibo Huang Jiajian Zhang and Xi-Yun Lu. Pinningdepinning mechanism of the contact line during evaporation of nanodroplets on heated heterogeneous surfaces: A molecular dynamics simulation. *Langmuir*, 35:6356–6366, 2019.

[4] C.W.M. van der Geld H.M.A. Wijshoff C. Diddens, J.G.M. Kuerten. Modeling the evaporation of sessile multicomponent droplets. *Journal of Colloid and Interface Science*, 487:426—-436, 2017.

[5] Todd F. Dupont Greg Huber Sidney R. Nagel Robert D. Deegan, Olgica Bakajin and Thomas A. Witten. Contact line deposits in an evaporating drop. *PHYSICAL REVIEW E VOLUME 62, NUMBER 1 JULY 2000*, 2000.

[6] Hua HuRonald G. Larson. Evaporation of a sessile droplet on a substrate. *The Journal of Physical Chemistry B*, 106(6):1334–1344, 2002.

[7] B. Haut A. Rednikov P. Colinet B. Sobac, P. Talbot. A comprehensive analysis of the evaporation of a liquid spherical drop. *Journal of Colloid and Interface Science*, 438:306–317, 2015.

[8] A.M. Cazabat G. Guéna, C. Poulard. Evaporating drops of alkane mixtures. *Colloids and Surfaces A: Physicochemical and Engineering Aspects Volume 298, Issues 1–2, 20 April 2007, Pages 2-11*, 2006.

[9] Christian Diddens. Detailed finite element method modeling of evaporating multi-component droplets. *Journal of Computational Physics*, 35:670–687, 2017.

[10] X. Fang R. Bhardwaj and D. Attinger. Pattern formation during the evaporation of a colloidal nanoliter drop: A numerical and experimental study. *New J Phys, vol. 11, Jul. 2009, doi: 10.1088/1367-2630/11/7/075020*, 2009.

[11] Weipeng ZhangJun YangGeorge K. Knopf. Numerical simulation of solvent evaporation in a reactive silver ink droplet deposited on a heated substrate. *ACS Omega*, 8(42):6356–6366, 2023.

[12] Maziar Raissi, Paris Perdikaris, and George E Karniadakis. Physics-informed neural networks: A deep learning framework for solving forward and inverse problems involving nonlinear partial differential equations. *Journal of Computational physics*, 378:686–707, 2019.

[13] Zhilu Lai, Charilaos Mylonas, Satish Nagarajaiah, and Eleni Chatzi. Structural identification with physics-informed neural ordinary differential equations. *Journal of Sound and Vibration*, 508:116196, 2021.

[14] Aleksei Sholokhov, Yuying Liu, Hassan Mansour, and Saleh Nabi. Physics-informed neural ode (pinode): embedding physics into models using collocation points. *Scientific Reports*, 13(1):10166, 2023.

[15] Tom Z Jiahao, M Ani Hsieh, and Eric Forgoston. Knowledge-based learning of nonlinear dynamics and chaos. *Chaos: An Interdisciplinary Journal of Nonlinear Science*, 31(11), 2021.

[16] Woojin Cho, Seunghyeon Cho, Hyundong Jin, Jinsung Jeon, Kookjin Lee, Sanghyun Hong, Dongeun Lee, Jonghyun Choi, and Noseong Park. Operator-learning-inspired modeling of neural ordinary differential equations. In *Proceedings of the AAAI Conference on Artificial Intelligence*, volume 38, pages 11543–11551, 2024.

[17] Yogesh Verma, Markus Heinonen, and Vikas Garg. Climode: Climate and weather forecasting with physics-informed neural odes. *arXiv preprint arXiv:2404.10024*, 2024.

[18] Taeyoung Kim and Myungjoo Kang. Approximating numerical fluxes using fourier neural operators for hyperbolic conservation laws. *CoRR*, 2024.

[19] Ravi G Patel, Nathaniel A Trask, Mitchell A Wood, and Eric C Cyr. A physics-informed operator regression framework for extracting data-driven continuum models. *Computer Methods in Applied Mechanics and Engineering*, 373:113500, 2021.

[20] Jonas A Actor, Xiaozhe Hu, Andy Huang, Scott A Roberts, and Nathaniel Trask. Data-driven whitney forms for structure-preserving control volume analysis. *Journal of Computational Physics*, 496:112520, 2024.

[21] et al. Lashkaripour, Ali. Machine learning enables design automation of microfluidic flow-focusing droplet generation. *Nature communications 12.1 (2021): 25*, 2021.

[22] Paul Arnov and Purbarun Dhar. Predicting sessile droplet evaporation kinetics via cascaded deep networks and tree-based machine learning approach. *Physics of Fluids 36.9 (2024)*, 2024.

[23] Kunihiko Taira Andalib, Sahar and H. Pirouz Kavehpour. Data-driven time-dependent state estimation for interfacial fluid mechanics in evaporating droplets. *Scientific Reports 11.1 (2021): 13579*, 2021.

[24] Maximilian Dreisbach, Elham Kiyani, Jochen Kriegseis, George Karniadakis, and Alexander Stroh. Pinns4drops: Convolutional feature-enhanced physics-informed neural networks for reconstructing two-phase flows. *arXiv preprint arXiv:2411.15949*, 2024.

[25] Ricky TQ Chen, Yulia Rubanova, Jesse Bettencourt, and David K Duvenaud. Neural ordinary differential equations. *Advances in neural information processing systems*, 31, 2018.

[26] Zongyi Li, Nikola Kovachki, Kamyar Azizzadenesheli, Burigede Liu, Kaushik Bhattacharya, Andrew Stuart, and Anima Anandkumar. Fourier neural operator for parametric partial differential equations. *arXiv preprint arXiv:2010.08895*, 2020.

[27] Lu Lu, Pengzhan Jin, Guofei Pang, Zhongqiang Zhang, and George Em Karniadakis. Learning nonlinear operators via deeponet based on the universal approximation theorem of operators. *Nature machine intelligence*, 3(3):218–229, 2021.

[28] DP Siregar, Johannes GM Kuerten, and CWM Van Der Geld. Numerical simulation of the drying of inkjet-printed droplets. *Journal of colloid and interface science*, 392:388–395, 2013.

[29] Meysam R Barmi and Carl D Meinhart. Convective flows in evaporating sessile droplets. *The Journal of Physical Chemistry B*, 118(9):2414–2421, 2014.

[30] Yohai Bar-Sinai, Stephan Hoyer, Jason Hickey, and Michael P Brenner. Learning data-driven discretizations for partial differential equations. *Proceedings of the National Academy of Sciences*, 116(31):15344–15349, 2019.

A Geometry of a Sessile Drop

A sessile drop is a spherical-cap shaped liquid solution in contact with a solid substrate. The surface of the liquid in contact with air is dependent on the surface energies of the liquid-gas-solid system. When modelling sessile drops, the radius of the droplet must be smaller than the capillary length defined by

$$l_{cap} = \sqrt{\frac{\gamma_{LG}}{\rho g}} \tag{19}$$

Which is dependent on the liquid-gas surface energy ($\gamma_L G$) and density of the solution (ρ). Capillary length is a comparison of the Laplace pressure to the hydrostatic pressure felt by the liquid and defines the length scale where Laplace pressure dominates. For a droplet of 99% water; this length is calculated to be 2.67 mm. There are four dimensions that define the geometry of droplets smaller than the capillary length [26]. These dimensions include the base radius (r_b), the sphere radius (R_S), the contact angle (θ_C), and the height of the sessile drop (h). There are only two independent dimensions with the four dimensions related by:

$$r_b = R_s \sin\theta_C \tag{20}$$

$$h = R_S(1 - \cos\theta_C) \tag{21}$$

These relations signify that two of the four variables are needed to provide the geometry of the drop. Using these dimensions, the volume of the drop is given by:

$$V = \beta\pi\frac{R_S^3}{3} \tag{22}$$

$$\beta = (1-\cos\theta_C)^2(2+\cos\theta_C) \tag{23}$$

B Analytical Evaporation model

Evaporation occurs when solvents like water and ethanol vaporize at the air-liquid boundary in the presence of vaporization pressure. For solvents such as water, a diffusion-limited model [5] can be used to model the rate of evaporation when the time it takes molecules to escape the interface is significantly shorter than the time it takes water vapor to diffuse into the atmosphere. The time scale for the saturation concentration to equilibrate is given by

$$t_{diff} = R^2/D_{vap} \tag{24}$$

Where this time is a function of drop radius (R) and vapor diffusivity (D_{vap}). For a water drop smaller than the capillary length this time is estimated to be $0.1s$. A diffusion limited model is applicable when this time scale is significantly less than the time for droplet evaporation. A diffusion-limited evaporation model is employed in this study.

A constant concentration has been observed at the liquid-air interface of water filled drops. This concentration is defined by a saturation pressure that is dependent on the temperature of the surrounding atmosphere (T). Saturation pressure of water is given by the Antoine equation shown as

$$P_{sat} = 10^{A-B/(C+T-273.15)}[mmHg] \tag{25}$$

with the constants A, B, and C determined experimentally for a particular solvent.

Saturation pressure is related to the concentration at the liquid-air interface by

$$c|_{\Gamma_1} = c_{sat} = P_{sat}/(R_s * T(r,z) * M_{H20}) \tag{26}$$

where concentration is calculated with the properties of molecular weight (M_{H2O}) and the specific gas constant (R_s).

The saturation concentration builds up around the surface and the mass flux of water is determined by how fast water vapor escapes from this saturated region. The mass flux of vapor at any point along the surface is given by

$$J_{evap} = D_{vap} * (\frac{\partial c}{\partial r}\cdot \boldsymbol{n_r} + \frac{\partial c}{\partial z}\cdot \boldsymbol{n_z}) \tag{27}$$

Following the model of Deegan et al. [5], the gradient of concentration in the air surrounding the drop is determined by solving the Laplace equation in the region bounded by the drop profile, substrate, and a large region of surrounding air ($r \to \infty$). The Laplace equation reads as:

$$\nabla^2 p(r,z) = 0 \tag{28}$$

With boundary conditions:

$$p|_\Gamma = p_{sat} \tag{29}$$

$$p(r \to inf) = RH * p_{sat} \tag{30}$$

$$\partial p|_{z=0} = 0 \tag{31}$$

The Laplace equation can be solved analytically by converting the cylindrical coordinates (r,z) to toroidal coordinates (α,β) [4] with the following conversion

$$\cosh\alpha = \frac{r^2\cos\theta + R_c\sqrt{R_c^2 - r^2(\sin^2\theta)}}{R_c^2 - r^2)} \tag{32}$$

$$N_{evap} = \frac{\pi\sqrt{2}(\cosh\alpha+\cos\theta)^{3/2}}{2\sqrt{2}(\pi-\theta)^2} \tag{33}$$

$$J_{evap} = N_{evap}\int_\alpha^\infty \frac{\tanh\frac{\pi x}{(2\pi-2\theta)}}{\cosh\frac{\pi x}{(2\pi-2\theta)}\sqrt{\cosh x - \cosh\alpha}}dx \tag{34}$$

For sessile drops, the introduction of a substrate creates a nonuniform evaporation along the droplet surface. Specifically, for droplets with a contact angle less than 90 degrees the evaporative flux at the solid-liquid contact line is much greater. The evaporation enhancement is linked to the greater probability of a water vapor molecule escaping at the drop corner as compared to the center of the drop [27]. There exists an analytical solution for the evaporative flux along the surface of a pure drop. Following the derivation of Deegan et al. [5], the An approximation of diffusion-limited evaporation along the droplet is given by

$$J/J^* = (\frac{1}{1-r/R_0})^{\frac{\pi-2\theta}{2(\pi-\theta)}} \tag{35}$$

With the evaporative flux normalized by

$$J^* = \frac{D_{vap}c_{sat}(1-RH)}{c_l R_0} \tag{36}$$

Where the normalized flux is dependent on the saturation concentration (c_{sat}), relative humidity (RH), vapor diffusivity (D_{vap}), and concentration of liquid water (c_l). As the contact angle decreases, the evaporative flux enhancement at the corner becomes greater.

From these mass flux solutions, the interface velocity cuased by evaporation is found using

$$w_e = -\frac{J_{evap}}{\rho}\sqrt{1+(\frac{\partial h}{\partial r})^2} \tag{37}$$

In the numerical model we add an $\varepsilon = 1e-6$ constant evaporation for stability.

C Experimental

C.1 Polymer Solution Preparation

TEMPO oxidized cellulose nanofibrils were purchased (Forest Products Lab, 2023-FPL-CNF-234) as a solution of 1.11 wt% CNF in water. Before use, the solution is stirred and centrifuged to ensure the solution used in experimentation is of homogeneous distribution and in a colloidal dispersion state. The desired quantity of 1.11 wt% solution is measured and diluted to the required mass percent. The diluted mixture is placed on a magnetic plate (Fisher Scientific, Isotemp FB30786163) and stirred using a magnetic stir rod at 600 RPM for 10 minutes. The stirred mixture was then centrifuged (ThermoFisher, Sorvall ST-8) at 3200 RPM for 3 minutes. The dispersed solution was chilled at 5 ºC until use to prevent gelation of the diluted solution.

C.2 Sessile Drop Tracking

The imaging set-up consists of a camera (PixeLink, PL-B741U) attached to a tube lens (Navitar, 1-60123 and 1-62831). This imaging set-up is focused on the surface of a hot plate (Fisher Scientific, Isotemp FB30786163) with a substrate of interest atop the hot plate surface. A backlight is stationed on the opposite side of the imaging set-up and directed at the tube lens. Figure 14 shows a depiction of the set-up and the resulting silhouette of an object placed on the hot plate is shown in Figure 14b.

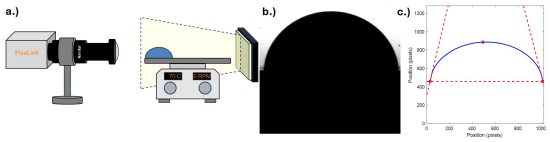

Figure 14: Experimental setup for tracking droplet evolution during evaporation. a) Schematic of droplet evolution measurement setup consisting of a tube microscope attached to a camera captures droplet evaporating on a hotplate that is backlit by a white light. b) Example image of a water droplet on a silicone surface at 20ºC. c) Dimensions extracted from image in MATLAB including diameter, height, and contact angles of drop.

A volume between 1.0-2.5 µL is measured using a micropipette (Eppendorf). The hot plate is brought to a specified temperature and, using a micromanipulator, the drop is brought into contact with the substrate. Imaging software (PixeLink Capture) is used to capture the evolution of the droplet over time. A custom image analysis script (MATLAB) was written to process the video and extract key parameters. A binarization scheme was developed to elucidate the drop boundary in every frame. The height, diameter, and contact angle are extracted; an example of the resulting measurements can be seen in Figure 14c.

D Simulated Data Supplementary results

For each trained Neural DrOps model, the learned evaporative flux was trained over several epochs until the loss function converged. For the data depicted in section 6.1, the evolution of the training and validation loss are depicted in Figure 15.

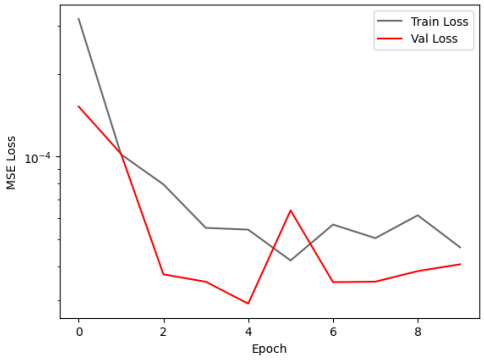

Figure 15: Training and validation loss for the learned evaporative flux using the Neural DrOps architecture.

An additional example of a simulated dataset is shown in Figure 18a. The Neural DrOps architecture was used to learn the evaporative flux and the predicted drop height evolution is shown in 18. Error between the predicted and true dataset shows decent prediction of evaporative flux with some error attributed to inadequacy of the numerical flow solver. Future work will be conducted to improve the ML architecture and numerical solver to improve agreement between the predicted and true dataset.

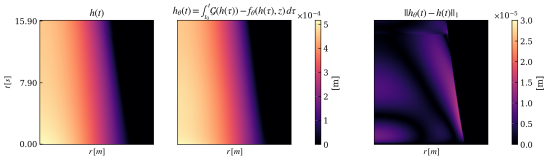

Figure 16: Training and validation loss for the learned evaporative flux using the Neural DrOps architecture.

E Experimental Data Supplementary Results

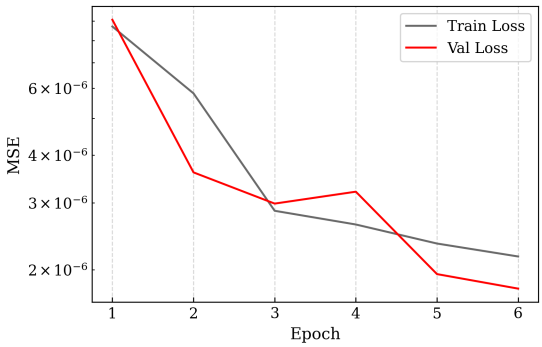

Figure 17: Training and validation loss for the learned evaporative flux using the Neural DrOps architecture.

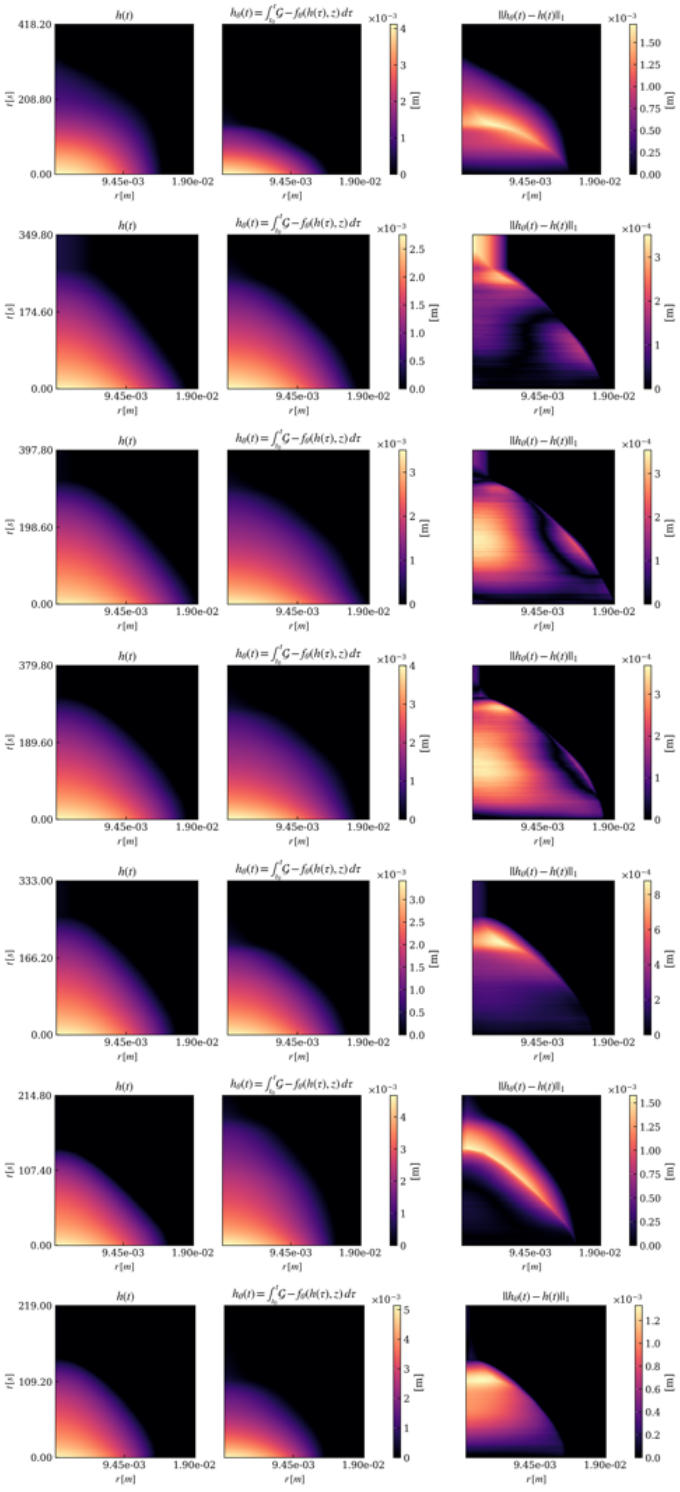

Figure 18: Training and validation loss for the learned evaporative flux using the Neural DrOps architecture.